Article

Effect of C$_2$H$_2$/H$_2$ Gas Mixture Ratio in Direct Low-Temperature Vacuum Carburization

Yeongha Song [1,2], Jun-Ho Kim [1], Kyu-Sik Kim [3], Sunkwang Kim [1,]* and Pung Keun Song [2,]*

[1] Dongnam Regional Division, Korea Institute of Industry Technology (KITECH), Namyangsan 1-gil 14, Yangsan 50635, Korea; yhsong1021@gmail.com (Y.S.); jhkim81@kitech.re.kr (J.-H.K.)

[2] Department of Materials Science and Engineering, Pusan National University, Busandaehak-ro 63beon-gil 2, Busan 46241, Korea

[3] Department of Materials Science and Engineering, Inha University, Inha-ro 100, Incheon 22212, Korea; kskim87@inha.edu

* Correspondence: skkim82@kitech.re.kr (S.K.); pksong@pusan.ac.kr (P.K.S.); Tel.: +82-55-367-9404 (S.K.); +82-51-510-2390 (P.K.S.)

check for updates

Abstract: The effect of the acetylene and hydrogen gases mixture ratios in direct low-temperature vacuum carburization was investigated. The gas ratio is an important parameter for producing free radicals in carburization. The free radicals can remove the natural oxide film by strong reaction of the hydrocarbons, and then thermodynamic activity can be increased. When the gas ratio was below one, carbon-supersaturated expanded austenite layers were formed on the surface of the AISI 316L stainless steel, which had a maximum carbon solubility up to 11.5 at% at 743 K. On the other hand, when the gas ratio was above one, the carbon concentration of the layers was low even if the process time was increased enough to reach the maximum carbon solubility. As a result, the carbon concentration underneath the surface was determined to be highly dependent on the gas mixture ratio of acetylene and hydrogen. In conclusion, it is necessary to restrict the ratio of acetylene and hydrogen gases in the total mixture of gases to form an expanded austenite layer with high carbon concentration in direct low-temperature vacuum carburization.

Keywords: direct surface activation; low-temperature vacuum carburization; expanded austenite; supersaturation; acetylene

1. Introduction

Austenitic stainless steel is used in a variety of industrial applications due to excellent corrosion resistance and mechanical properties, as well as especially low-temperature toughness. However, it has poor wear resistance and hardness when employed in applications requiring high mechanical properties. Meanwhile, surface hardening technologies such as nitriding, carburizing, and nitrocarburizing have been extensively studied [1]. However, austenitic stainless steel has a limitation in that it requires a low temperature in the surface hardening treatment as a high temperature would reduce its corrosion resistance. Therefore, low-temperature carburization was proposed and commercialized to enhance surface mechanical properties such as hardness and wear resistance, while maintaining the inherent corrosion resistance of austenitic stainless steel [2–7]. In this process, carbon atoms penetrate into the austenite matrix to form a supersaturated solid solution [8].

The natural oxide film on the austenitic stainless steel prevents the penetration of carbon atoms into the austenite matrix, and the solubility of carbon is considerably decreased [9,10]. Thus, an additional process is required to remove and/or convert the natural oxide layer on the surface in order to improve the mechanical properties of austenitic stainless steel in low-temperature

carburization. Surface activation has been researched to improve the efficiency of carbon atoms penetration into austenitic stainless steel since the 1960s. The traditional surface activation methods can be classified as follows: (a) removal of the oxide layer with a chloride resin [11], a metal halide salt bath [12], and halogen gases [13], (b) easy penetration of carbon atoms using thin iron films [14], and (c) breakage of the oxide layer by high-energy ion bombardment such as plasma sputtering [15]. Compared with the traditional methods, the recently developed method that involves exposure of the steel to a halogen gas atmosphere containing gases such as HCl, NF_3, and urea acid, has been commercially applied [2,7,13].

However, growing environmental problems have necessitated the development of alternative ways that employ low toxicity methods. Recently, acetylene gas (C_2H_2) as a carbon source was employed to remove the natural oxide layer and improve the carburization efficiency in carburization [16–18]. The mechanism of carburization in acetylene is as follows: first, adsorption and decomposition of C_2H_2 gas on the solid surface takes place at a certain temperature and, subsequently, the developed radicals generate carbon species [19,20] that are soluble in iron. Simultaneously, the natural oxide film is removed by the activation energy of the radical gas [20].

Low-temperature carburization with C_2H_2 gas has been studied with regard to the influence of change of process temperature and time on the activity and diffusion rate [17,21,22]. In carburization, C_2H_2 gas even in small amounts causes sufficient reaction for carburization in vacuum, and leads to a decrease in the oxygen partial pressure, so that the natural oxide layer is naturally decomposed [17,22]. Owing to the characteristics of acetylene in the low-temperature regime, carburization in vacuum was proposed to control soot and/or metal dust easily [16]. Another study observed the change in carbon activity and the oxygen partial pressure according to the ratio of the process gas [17].

Nevertheless, there is lack of studies on the effect of the C_2H_2 gas ratio to the total process gases in low-temperature vacuum carburization. Therefore, theoretical and experimental studies are required from this aspect, because the process gas ratio, which is an important experimental parameter that affects the carburization efficiency, leads to the production of radicals that cause strong reaction of the hydrocarbons, and determine the thermodynamic activity by degree of vacuum and gas ratio [16,20].

In this study, we focused on the carburization effects of the ratio of C_2H_2 and H_2 gases in a low-temperature vacuum carburizing process. After the treatment, the carburization thickness, carbon concentration, and hardness depth profiles were analyzed, following which the experimental data were compared with the calculated data based on a previously reported numerical study [4]. On the premise of validity, the influences of gas ratio on the carbon solubility (para-equilibrium carbon concentration) and the critical ratio of C_2H_2 and H_2 mixture gases was confirmed by an increase in carburization time and the change of the gas ratio during the process.

2. Materials and Methods

In this study, numerical simulations were carried out by computational calculation before direct low-temperature vacuum carburization to obtain a uniform carburization layer thickness of at least 20 μm. The numerical simulations were based on the finite difference method, where Fick's 2nd law was discretized as a finite difference approximation in the dimensions of penetration depth of x (μm) and treatment time of t (s) [23,24]. The Crank–Nicolson algorithm was used for the computational calculations. The boundary conditions for AISI 316L stainless steel (ASS) were fixed; the maximum carbon solubility C_{max} at the gas-metal interface was selected at 11.5 at% owing to being most suitable considering the alloy elements of ASS used in this study [7]. The diffusion coefficient D was 4.5×10^{-5} μm²/s at 743 K (470 °C) at infinite dilution, according to the value obtained by Agarwala et al. [25]. However, other studies [23,24] indicate that D depends on the concentration during diffusion of the dissolved carbon atoms in the metal. Therefore, D needs to be calculated by changing the concentration dependence of the diffusion coefficient (D'). D' can be calculated from the well-known Equation (1).

$$D' = D \, Exp\left(k \frac{C}{C_{max}}\right) \tag{1}$$

The ASS rods were round bar and cut to dimension of $\Phi31$ mm $\times$ T7 mm to prepare the test samples. The chemical compositions of the samples are presented in Table 1. Before carburization, the samples were annealed for 3 h at 1353 K. They were then polished with silicon carbide papers (180–2000 grit), followed by mechanical polishing in the final step with a 1 µm diamond suspension to achieve a mirror-like surface finish. Finally, the surface contaminations were removed by separate ultrasonic cleaning in acetone and ethanol solution.

Table 1. Chemical compositions of commercial grade AISI 316L.

Material	C	Si	Mn	P	S	Ni	Cr	Mo	Cu	Fe
AISI 316L	0.02	0.48	1.8	0.03	0.02	10.03	16.66	2.05	4.3	Bal.

Direct low-temperature vacuum carburization was performed in a commercial vacuum carburizing furnace (VH556-10, Rübig, Wels, Austria), for which detailed experimental conditions are shown in Table 2. The furnace chamber was evacuated to 1 Pa for 6 h at 743 K before the tests in order to remove the impurities in the furnace and stabilize the samples. High purity acetylene gas (C_2H_2; 99.90%) and high purity hydrogen gas (H_2; 99.999%) were used as the process gases. They were mixed in a gas ratio of 0.05, 1, 5, and 10 and introduced during the test. The total amount of the process gases was maintained constant at 300 standard liters per hour (SLH), with identical flow rate in all processes. The carburization was performed at a working pressure of 800 Pa and temperature of 743 K. After carburization, the samples were cooled to 473 K in 60 s with 5 bar of nitrogen gas to prevent any sudden irregular changes; the samples reached room temperature in 10 min.

Table 2. Experimental conditions of direct low-temperature vacuum carburization.

Exp. No	Gas Mixture Ratio	Gas Composition	Time (h)	Temp (K)	Pressure (Pa)
A-1	0.05	0.05 C_2H_2–0.95 H_2	14		
A-2	1	0.5 C_2H_2–0.5 H_2	14		
A-3	5	0.83 C_2H_2–0.17 H_2	14		
A-4	10	0.91 C_2H_2–0.09 H_2	14		
A-5	1	0.5 C_2H_2–0.5 H_2	42	743	800
A-6	10	0.91 C_2H_2–0.09 H_2	42		
A-7	0.05	0.05 C_2H_2–0.95 H_2	3.5		
A-8	0.05	0.05 C_2H_2–0.95 H_2	7		
A-9	0.05 → 10	0.05 C_2H_2–0.95 H_2 0.91 C_2H_2–0.09 H_2	7 → 7		

All samples were analyzed after carburization as follows. The samples were etched in aqua regia for 10 min and observed by optical microscopy (OM) using a Nikon Eclipse LV 150NL. The micro Knoop hardness was measured using a Mitutoyo HM210 hardness tester with a load of 98 mN for 15 s. X-ray diffraction (XRD) analysis was used to identify the phase in the conventional symmetric Bragg-Brentano geometry, with monochromatic X-ray provided by Cu-Kα radiation, using the Ultima 4 diffractometer (Rigaku, Japan). The carbon concentration and thickness of the carburization layer were determined with the conditions of 700 V, 30 mA, 20 points/s and cal. factor 0.7 by glow discharge optical emission spectroscopy (GDOES) using GDS850A spectrometer (LECO, USA).

3. Results

In this study, direct low-temperature vacuum carburization was conducted to investigate the effects of the C_2H_2 and H_2 gases mixture ratios on the formation of the carburization layer, which is well known as expanded austenite layer. The ratios of C_2H_2 gas to the total gases and the process time were changed. The other conditions were constant at both working pressure 800 Pa and temperature 743 K in all carburization treatments as mentioned in the experimental method.

Figure 1 shows the cross-sectional OM images of ASS samples carburized at various gas mixture ratios of 0.05, 1, and 10. The expanded austenite layer clearly separated from the substrate can be observed in Figure 1a,b, cross-sectional images of samples carburized at the conditions of A-1 and A-4, respectively. While an expanded austenite layer was uniformly formed at the conditions of A-1, it was not uniform at the conditions of A-4, in which a thickness deviation of 5 μm was observed. In Figure 1c, for which the sample was carburized at the conditions of A-5, there is an expanded austenite layer with a uniform thickness of about 35 μm. On the other hand, the expanded austenite layer in the sample carburized at the conditions of A-6 showed a maximum thickness of about 30 μm and a wavy (non-uniformed) pattern with a thickness variation of 15 μm.
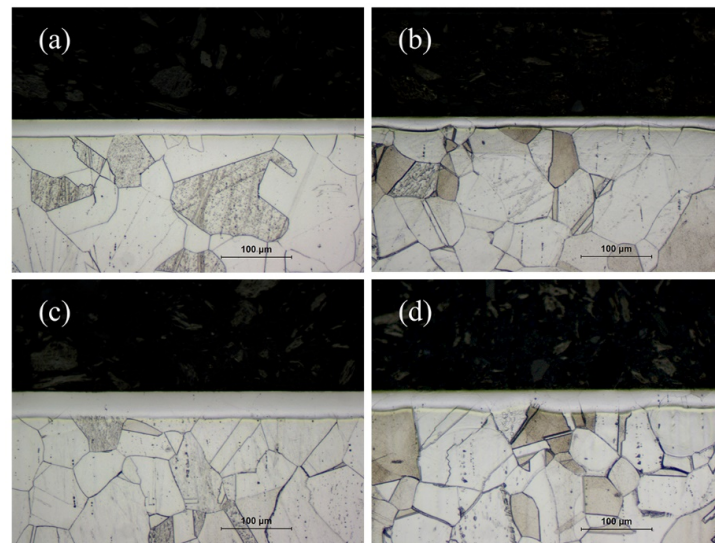

Figure 1. Cross-sectional optical microscope images of the AISI 316L stainless steel (ASS) carburized with various gas mixture ratios of (**a**) 0.05 and (**b**) 10 for 14 h, and (**c**) 1 and (**d**) 10 for 42 h.

Figure 2 shows numerical simulation and experimental data obtained by GDOES analysis. In Figure 2a, the carbon concentration depth profiles were obtained from the calculated and experimental data of the ASS samples carburized for 14 h at gas ratios of 0.05, 1, 5, and 10. To obtain the calculated data, the boundary conditions stated in Section 2 were applied to the diffusion equation. Further, the concentration dependence of the diffusion coefficient was calculated using Equation (1). The simulated carbon concentration depth profiles reported in two studies [24,25] presented a best fit, corresponding to $k = 5.0$ at Equation (1) [4,24]; however, the best fit profile obtained for the experimental data corresponds to $k = 2.0$ in this study. The difference of k value as compared to others results may be because the carbon concentrations effectively reach the para-equilibrium solubility limit at the beginning of the treatment owing to the removal of the natural oxide film before the low-temperature vacuum carburization [24,25]. Moreover, there is a difference between the calculated and experimental data in that the carbon concentration underneath the surface is slightly higher than that of the maximum carbon solubility of 11.5 at%. This is attributed to protrusion of a large amount of carbon, sticking and/or absorbed to the surface at the beginning of the sputtering, which is inherent in GDOES, which was used to measure the carbon concentration [26]. Therefore, the *y*-axis intercept, which is the value at the *y*-axis obtained by extending a straight line toward it from the slope at the point 1 μm where the high concentration of the surface abruptly drops, is about 11.5 at% and may be considered as the surface concentration in this study. The maximum carbon concentration was both 11.5 at% for the conditions of A-1 and A-2, and gradually decreased toward the depth, equal to the substrate concentrations of 0.1 at% at a depth of 23 μm. On the other hand, the carbon concentration showed maximum values of 9.8 and 7.5 at% underneath the surface of the sample carburized at the conditions of A-3 and A-4, and were equal to that of the substrate at a depth

of about 21.3 and 17 µm, respectively. In other words, compared with the surface carbon concentration obtained at the conditions of A-4, A-3 was high but below the maximum carbon solubility of 11.5 at%. Figure 2b shows the calculated and experimental data of the samples carburized at the conditions of A-5 and A-6. The calculated data agree with the experimental result obtained for the conditions of A-5. The maximum carbon concentration appeared at 1 µm underneath the surface, and the concentration was sharply decreased from about 20 µm; the concentration profiles were almost similar in shape to those obtained for the conditions of A-2.
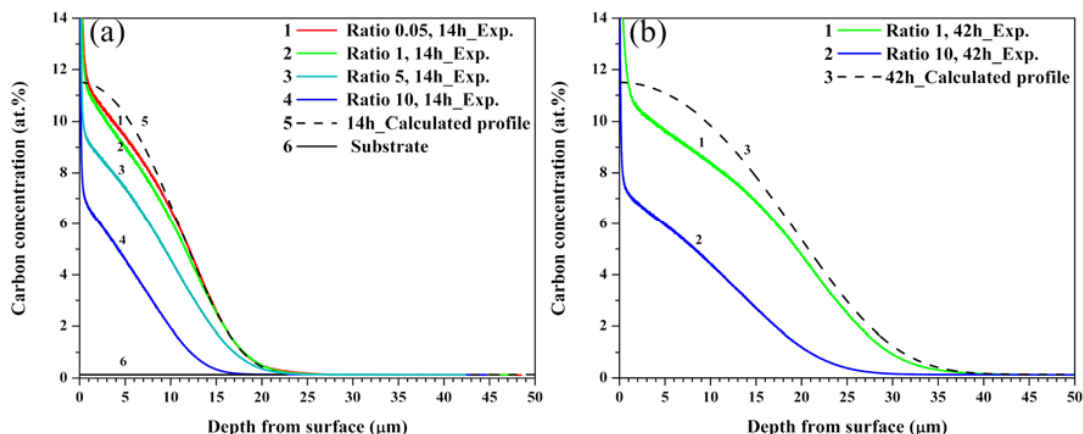

Figure 2. Glow discharge optical emission spectroscopy (GDOES) carbon concentration depth profile of the ASS carburized for (**a**) 14 h and (**b**) 42 h.

Figure 3 presents the crystal structure of the ASS samples carburized with various gas mixture ratios of 0.05, 1, 5, and 10, as obtained by XRD analysis. In Figure 3a, strong intensity peaks of γ-Fe phases, and two preferred orientations of (111) and (200), were observed. The peaks of the untreated sample occurred at 2θ values of 43.44° and 50.58°. However, the peaks of all the carburized samples shifted toward a lower angle direction as compared to those of the untreated sample. For the conditions of A-4, the peaks of (111) and (200) were found at 2θ values of 42.77° and 49.39°, respectively, whereas, for the conditions of A-1, these peaks shifted the most, to 42.35° and 48.96°, respectively. The shift of the peak implies that the FCC (Face Centered Cubic) lattice expanded with an increase in the lattice constant, a, which was 0.3606 nm for the untreated sample and 0.3694 nm for the conditions of A-2.
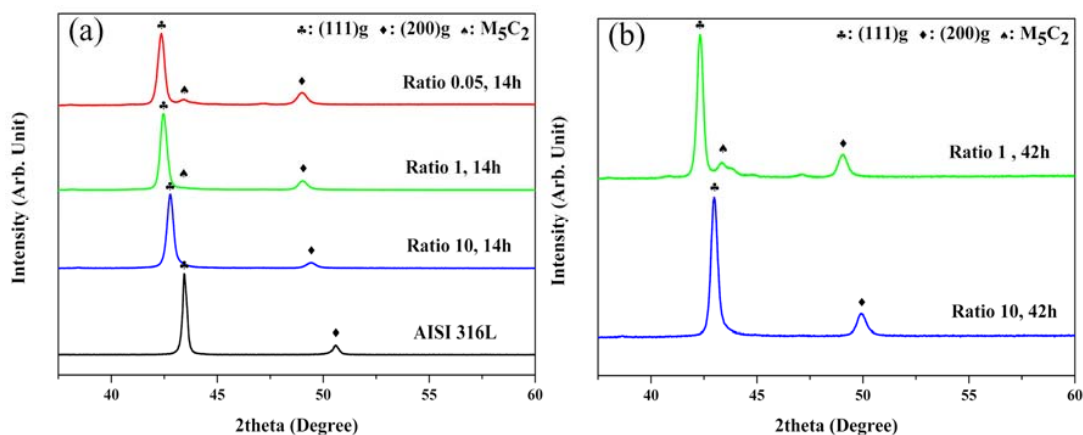

Figure 3. X-ray diffraction (XRD) patterns obtained from the ASS samples carburized for (**a**) 14 h and (**b**) 42 h.

Furthemore, a weak intensity peak belong to a second phase was observed at 2θ = 43.33°, which corresponds to a plane spacing d of ≈ 0.2086 nm, for the conditions of only A-1 and A-2, where the maximum carbon concentration was about 11.5 at%. Therefore, it can be presumed that the phase has a crystal structure of M_5C_2, the Hägg carbide [4,27] which is known to form at higher carbon concentration of 11 at% in the previous reported reference [4]. In the XRD results of Figure 3b, the (111) peak of the XRD result of the sample carburized at the conditions of A-5 was slightly shifted by 0.2° toward a lower angle than that obtained in the result at conditions of A-2, and the Hägg carbide peak was also observed with slightly increased intensity. In the conditions of A-6, however, XRD results were obtained which were almost the same as those of the sample carburized at the conditions of A-3. That is, the (111) peak was observed at approximately the same position as the conditions of A-3 and A-5, but the peak of M_5C_2 was not detected.

In Figure 4a, the maximum hardness values of the samples carburized at the conditions of A-1 and A-2 were 812 and 747 $Hk_{0.01}$ at 2 μm, respectively; however, both hardness values were sharply decreased from about 8 μm, and equaled the substrate hardness values of 150 $Hk_{0.01}$ at 22 μm. On the other hand, the maximum hardness values of the sample carburized at the condition of A-3 and A-4 were 560 and 480 $Hk_{0.01}$; these values rapidly decreased from about 2 μm and became 150 $Hk_{0.01}$ at 17 μm. As shown in Figure 4b, the maximum hardness value of the sample carburized at the conditions of A-5 was 890 $Hk_{0.01}$ at 2 μm, and remained above 550 $Hk_{0.01}$ until about 20 μm, and finally, equaled the substrate hardness value at about 35 μm. In the case of the sample carburized at the conditions of A-6, however, the maximum hardness value was slightly increased to 550 $Hk_{0.01}$ as compared with the sample carburized at the conditions of A-4 (See Figure 4b: error bars denote the standard error for the mean of the hardness values in the expanded austenite layer with wide range deviations of ±100–200 $Hk_{0.01}$, obtained by averaging the hardness values of each thin and thick layer to calculate the standard error.).

The values of the maximum carbon concentration and hardness of Figures 2 and 4 did not significantly change as compared to those with the sample carburized for 14 h, although carburization was carried out for a longer duration. However, the carbon concentration and hardness below the maximum value area were high for the condition of 42 h, as compared to carburization for 14 h. Thus, it was confirmed that the hardness depth profiles show a very similar behavior to the carbon concentration depth profiles.
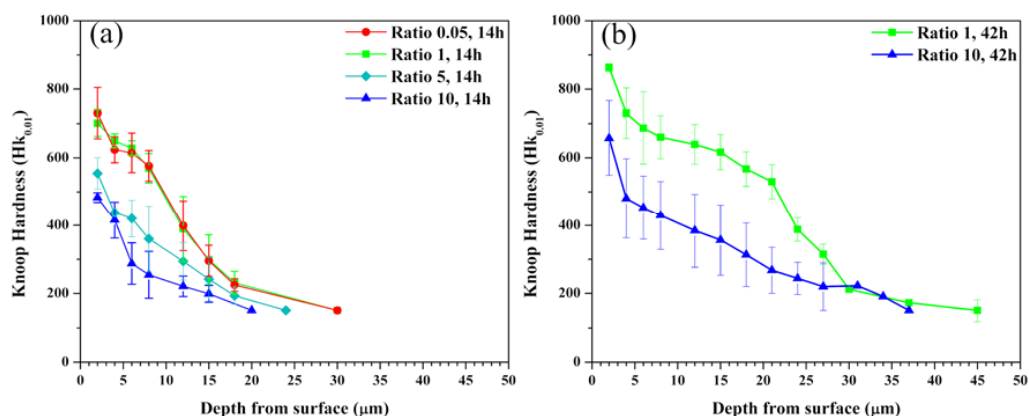

Figure 4. Hardness depth profile of ASS samples carburized for (**a**) 14 h and (**b**) 42 h.

Figure 5 shows the cross-sectional microstructure images, carbon concentration, and hardness depth profiles for the samples carburized for 3.5 h; (a) A-7, 7 h; (b) A-8, for 7 h at gas ratio of 0.05 followed by for 7 h at gas ratio of 10; (c) A-9. Figure 5a–c shows the cross-sectional images of samples carburized at the three aforementioned conditions; the thickness values of the expanded austenite

layers are 13, 15, and 17 µm, respectively. They are almost similar to those obtained from the carbon concentration depth profiles in Figure 5d and hardness depth profiles in Figure 5e.

The carbon concentrations underneath the surface of the samples carburized at the conditions of A-7 and A-8 were similar, at about 11.5 at% (Figure 5d). For the conditions of A-9, however, the carbon concentration underneath the surface was decreased from the high concentration of 11.5 at% obtained after the sample carburized at the conditions of A-8, and was similar to that obtained at the conditions of A-4. Comparing the results obtained at the conditions of A-4 and A-9, it can be seen that the carbon concentration was slightly higher for the latter, 5 µm. This result is also observed in the hardness depth profiles in Figure 5e for the three aforementioned conditions. The maximum hardness was 680 $Hk_{0.01}$ in the sample carburized at the conditions of A-8, and then drastically decreased to that of substrate. For the samples carburized at the conditions of A-4 and A-9, all hardness values were similar, exhibiting a lower maximum at 480 $Hk_{0.01}$, as compared to the sample carburized at the condition of A-8. Nevertheless, the thickness of the expanded austenite layer for the sample carburized at A-9 was about 20 µm, and almost equal to that for the sample carburized at the conditions of A-4.
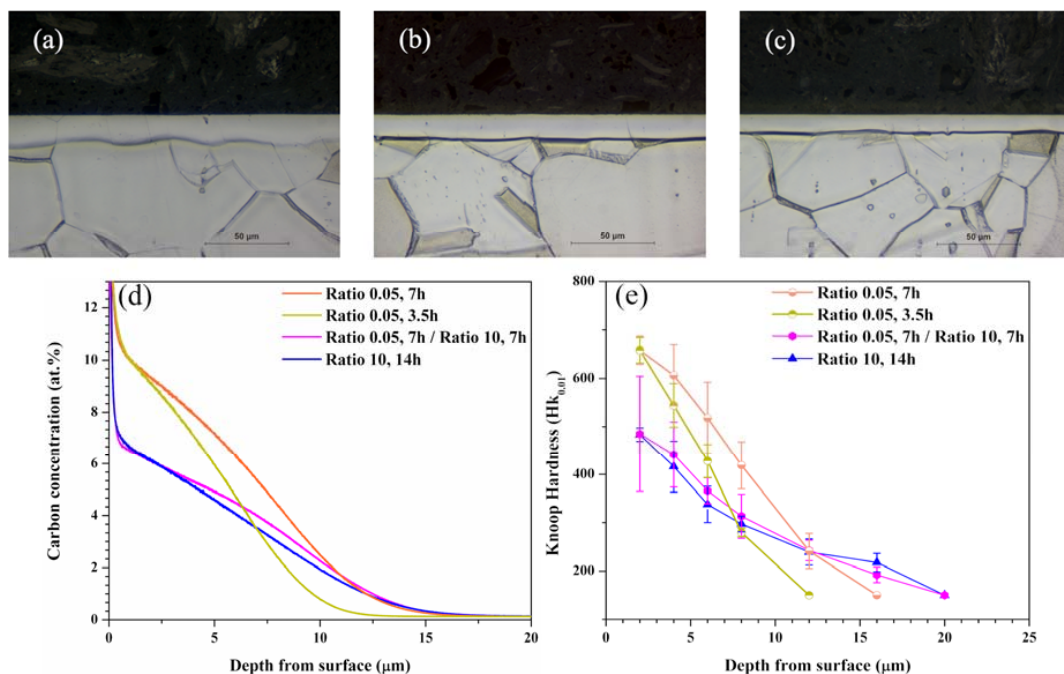

Figure 5. Cross-sectional optical microscope image of ASS samples carburized using gas mixture ratio of (**a**) 0.05 for 7 h followed by 10 for 10 h, (**b**) 0.05 for 7 h and (**c**) 0.05 for 3.5 h, (**d**) GDOES carbon concentration depth profile of ASS samples carburized by gas mixture ratio 0.05 for 7 h, ratio 0.05 for 7 h followed by ratio of 10 for 10 h and ratio of 14 for 10 h and, (**e**) hardness depth profile of ASS sample carburized by gas mixture ratio of 0.05 for 7 h, ratio of 0.05 for 3.5 h, ratio of 0.05 for 7 h followed by ratio of 10 for 7 h and ratio of 10 for 14 h.

4. Discussion

As shown in the experimental results, the yield of the expanded austenite layer depends on the gas ratio used in the direct low-temperature vacuum carburization employing acetylene gas. The maximum carbon concentration of samples carburized at the conditions of A-1 and A-2 were similar, at 11–12 at% [4,28], and the thickness values of the expanded austenite layer were also similar, at 22 µm, in this study. On the other hand, the carbon concentration and the thickness of the layer at the conditions of A-3 and A-4 were significantly lower than those at the lower gas ratios. In particular, for the conditions of A-4, the thickness of the expanded austenite layer was uneven, in a range of

13–18 μm with large standard error. Compared with that, the thickness of the expanded austenite layer for the conditions of A-3 was about 21 μm, which is further increased.

Acetylene is known to adsorb on the surface of a metal base material [20] and decompose into hydrogen and carbon, which is diffused and dissolved at the interstitial site. In this study, however, the carbon concentration was the lowest at the conditions of A-4, which has the highest amount of acetylene, even though there are many more carbon species which can dissolve in the substrate. This implies that an adequate amount of hydrogen is necessary at a certain temperature in low-temperature vacuum carburization employing C_2H_2 gas [20,29]. This observation is consistent with a study wherein despite the expected observation that the flow of high gas ratio C_2H_2 with nearly infinite carbon activity would increase the carbon concentration in ASS, the actual carburization efficiency was very low [16]. This lowering of the carburization efficiency for a high ratio of C_2H_2 can be expected as follows [16,17]: (a) it is difficult to increase to the para-equilibrium carbon solubility limit due to a lack of free radicals generated, which depends on the amount of the H_2 gas introduced, (b) the transfer of soluble carbon species from the gas atmosphere into the solid is hindered by the soot and metal dust formed due to the high activity of C_2H_2 gas.

In this study, the expanded austenite layers were uniformly formed on the surface except for some specific conditions. On the other hand, the soot with dark grayish color was produced after low-temperature vacuum carburization under all of the process conditions as shown in Figure 6, because the acetylene activity was as high as about 10^3–10^5 even in vacuum. Accordingly, it is not a necessary to consider that the interruption of the transfer of soluble carbon species by soot and metal dust is the reason for deteriorating carburizing efficiency mentioned in (b) because soot and metal dust were formed even under the conditions with the uniform layer. Therefore, the reduction of the carburization efficiency at the conditions of A-4 was probably the result of decreased radicals owing to the lack of hydrogen gas. Due to lack of free radicals, the natural oxide layer is not completely removed or the para-equilibrium carbon concentration is lower; hence, carbon is unevenly dissolved in the austenite matrix and consequently, the carbon concentration profile in the entire carburization layer may not increase. Generally, the carburization layer is formed via concentration-dependent diffusion as a function of $\sqrt{Dt}$. In the bulk material carburized at low temperature, therefore, the heterogeneous solid solution of carbon atoms may have formed (or may have formed in the initial diffusion regime) owing to limited expansion of the lattice by the surrounding one, different diffusion path, or a different carbon diffusion rate depending on the crystal orientation [30,31]. At that time, if the carbon species continue to get introduced from the surface, the ASS will be able to continuously maintain the maximum para-equilibrium carbon concentration, and therefore the internal carbon concentration can be gradually increased as the carbon continues to diffuse inward. However, if the natural oxide layer is not completely removed or the para-equilibrium carbon concentration is lowered, the diffusion rate is inevitably lower due to the lack of carbon species introduced from the interface of the gas and solid. Therefore, the expanded austenite layer in the conditions of A-4 had a relatively low carbon concentration compared to that in the other conditions, despite carburization for the same time.
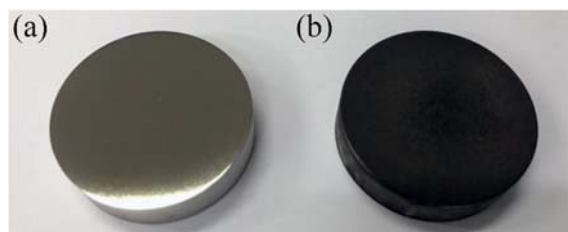

Figure 6. The photo-images of ASS samples (**a**) untreated and (**b**) low-temperature carburized.

Carburization was carried out for 42 h in order to confirm whether the carbon concentration in the expanded austenite layer increased with the process time, despite the lack of free radicals; the results

are shown in Figure 3. At conditions of A-5, adequate free radicals were produced by sufficient hydrogen gas. Therefore, the sample acquired a carbon concentration and a thickness of the expanded austenite layer almost similar to the maximum carbon solubility of 11.5 at% [28] and the predicted theoretical result, respectively. For the conditions of A-6, however, the thickness of the expanded austenite layer increased to a maximum of 30 μm, but was not constant and had a large deviation, as shown in the cross-sectional OM image. Moreover, the maximum carbon concentration was 7.5 at%, compared with the result obtained at the conditions of A-4. Therefore, the para-equilibrium carbon concentration did not increase with the process time when the numbers of free radicals generated by the small amount of hydrogen gas ratio in the total process gases was small. Thus, carbon species are continuously supplied only at a specific concentration by the generated free radicals under each process condition, even if the process time increases.

The results obtained by changing the gas ratio in-process (Figure 5) show that the gas ratio has a great influence on the formation of radicals. For conditions of A-8, the surface may have been activated relatively quickly by the number of free radicals, following which the carbon atoms diffused through the surface to the substrate; thus, the expanded austenite layer was thin with a high hardness value, with a uniform and maximum carbon concentration of about 11 at%. On the other hand, when the number of free radicals was reduced by changing the gas ratio from 0.05 to 10, the result was similar to that for the sample carburized at the conditions of A-4, because the carbon concentration at the interface between the gas and metal decreased with a decrease in the free radicals.

Based on these results, Figure 7 shows a schematic of the variance in the carbon concentration profile due to changes in the para-equilibrium carbon concentration according to the gas ratio. In Figure 7a,b, the influence on the formation of the expanded austenite layer by the difference in the para-equilibrium carbon concentrations, $C_{eqs-g}(0.05)$ at gas ratio of 0.05 and $C_{eqs-g}(10)$ at gas ratio of 10, is shown. When $C_{eqs-g}(0.05)$ is high, the surface carbon concentration $C_s(0.05)$ reaches the maximum value in a short time, owing to the high activity of acetylene, whereas, when the carburization time increases, the carbon is diffused in the depth direction while maintaining the surface concentration. For a gas ratio of 10, On the other hand, the carbon concentration $C_s(10)$ underneath the surface becomes lower due to insufficient amount of radicals, and does not change even with an increase in the process time; only diffusion occurs, as shown in the experimental results in Figure 5d.
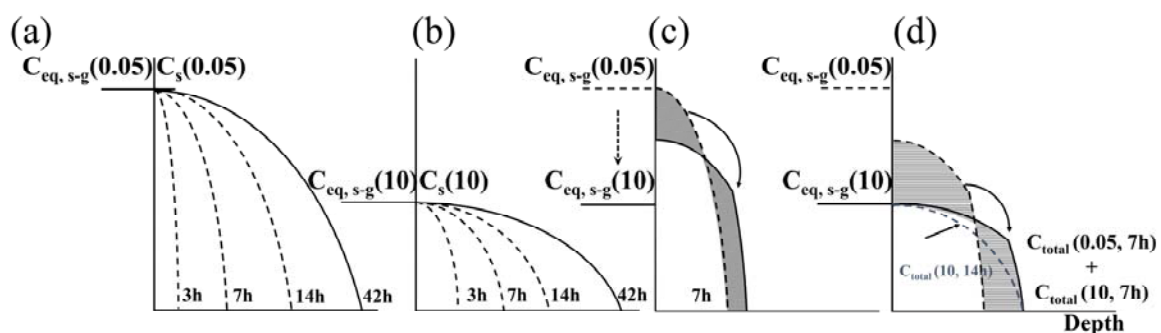

Figure 7. Schematic illustrations of the carbon concentration profiles at gas ratio of (**a**) 0.05 and (**b**) 10, and the variance of the profile due to the difference of the para-equilibrium carbon concentration when the gas ratio was changed from 0.05 to 10: (**c**) the step in which the carbon atoms on the surface side diffused toward the substrate, and (**d**) the step where the surface carbon concentration and the para-equilibrium carbon concentration at gas ratio of 10 are equal.

As shown in Figure 7c,d, after carburization, although the gas ratio was only changed with the same carburization time, the carburization depth and the surface carbon concentration were similar. It is anticipated that if $C_{eq,s-g}(10)$ is decreased from $C_{eq,s-g}(0.05)$, the carbon atoms dissolved in the surface by carburization at a gas ratio of 0.05 only diffuse into the substrate, because $C_s(0.05)$ is higher than $C_{eq,s-g}(10)$, and no additional carbon atoms are supplied through the interface from the gas

atmosphere. As shown in Figure 7d, however, the difference between the carbon concentration profiles is as follows: When the gas ratio is changed during the process for one in two carburization conditions, the expanded austenite layers at both conditions have the same thickness; however, there are deviations in the middle parts of the carbon concentration profiles. This means $C_{total}(0.05, 7 \text{ h})$, which is the total carbon concentration in the expanded austenite layer formed by carburization for 7 h at a gas ratio of 0.05, is higher than $C_{total}(10, 7 \text{ h})$, which is the total carbon concentration in the expanded austenite layer formed by the carburization for 7 h at a gas ratio of 10. Finally, when $C_s(10)$ is lower than $C_{eq,s-g}(10)$, the carbon atoms are introduced from outside the gas and are continuously diffused toward the substrate.

5. Conclusions

In the present study, the effect of acetylene and hydrogen mixture gas ratios in direct low-temperature vacuum carburization was investigated. The results can be summarized as follows:

AISI 316L stainless steel was carburized with acetylene and hydrogen gas mixture ratio of 0.05, 1, 5, and 10 at 800 Pa for 14 h at 743 K, these results showed that an increase of the acetylene gas ratio led to lower surface carbon concentration and thickness of the expanded austenite layer. This lowering of the carburization efficiency for the direct low-temperature vacuum carburization, even though the amount of acetylene is greatly increased, can be explained as follows. The efficiency of the free radicals generated by acetylene decomposition depends on the gas mixture ratio.

The main conclusions are as follows:

- The theoretical results based on the diffusion model with concentration dependence of the diffusion coefficient were in agreement with the experimental results of AISI 316L stainless steel carburized at the gas ratio of 0.05 and 1 at 743 K. The calculated result presented the best fit corresponding to $k = 2$.
- While the gas mixture ratio of acetylene increases, the efficiency of carburization decreases, which also depends on the amount of hydrogen gas in the total gases. That is, when the amount of hydrogen is smaller than the gas ratio of one in this study, the generation of free radicals is reduced. As a result, the supplement of carbon atoms, which affect directly the natural oxide film and/or carburization, is significantly reduced.
- When the gas ratio of acetylene to hydrogen was changed during the carburization process, the thickness of the expanded austenite layer and carbon concentration showed the same results under the two conditions of the carburization processes of changing the gas ratio of 0.05 to 10 and maintaining the gas ratio of 10. In other words, the results obtained by maintaining a gas ratio and changing the gas ratio during the carburization process are very similar, if the process time is the same. These results are explained in detail by the model shown in Figure 7.

Author Contributions: Y.S., S.K., and P.K.S. conceived and designed the experiments; K.-S.K. and S.K. performed the experiments; Y.S., J.-H.K., S.K., and P.K.S. analyzed and discussed the data; Y.S., S.K., and J.-H.K wrote the paper; S.K., and P.K.S. Review & Editing.

Conflicts of Interest: The authors declare no conflict of interest.

References

1. Rong, D.S.; Gong, J.M.; Jiang, Y. Thermodynamic Simulation of Low Temperature Colossal Carburization of Austenitic Stainless Steel. *Procedia Eng.* **2015**, *130*, 676–684. [CrossRef]
2. Collins, S.R.; Williams, P.C.; Marx, S.V.; Heuer, A.H.; Ernst, F.; Kahn, H. Low-Temperature Carburization of Austenitic Stainless Steels. In *ASM Handbook, Volume 4D: Heat Treating of Irons and Steels*; ASM: Almere, The Netherlands, 2014; Volume 4, pp. 451–460, ISBN 978-1-62708-066-8.

3. Tsujikawa, M.; Yoshida, D.; Yamauchi, N.; Ueda, N.; Sone, T.; Tanaka, S. Surface material design of 316 stainless steel by combination of low temperature carburizing and nitriding. *Surf. Coat. Technol.* **2005**, *200*, 507–511. [CrossRef]

4. Cao, Y.; Ernst, F.; Michal, G.M. Colossal carbon supersaturation in austenitic stainless steels carburized at low temperature. *Acta Mater.* **2003**, *51*, 4171–4181. [CrossRef]

5. Ernst, F.; Avishai, A.; Kahn, H.; Gu, X.; Michal, G.M.; Heuer, A.H. Enhanced carbon diffusion in austenitic stainless steel carburized at low temperature. *Metall. Mater. Trans. A Phys. Metall. Mater. Sci.* **2009**, *40*, 1768–1780. [CrossRef]

6. Martin, F.J.; Natishan, P.M.; Lemieux, E.J.; Newbauer, T.M.; Rayne, R.J.; Bayles, R.A.; Kahn, H.; Michal, G.M.; Ernst, F.; Heuer, A.H. Enhanced corrosion resistance of stainless steel carburized at low temperature. *Metall. Mater. Trans. A Phys. Metall. Mater. Sci.* **2009**, *40*, 1805–1810. [CrossRef]

7. Michal, G.M.; Ernst, F.; Kahn, H.; Cao, Y.; Oba, F.; Agarwal, N.; Heuer, A.H. Carbon supersaturation due to paraequilibrium carburization: Stainless steels with greatly improved mechanical properties. *Acta Mater.* **2006**, *54*, 1597–1606. [CrossRef]

8. Bell, T. Surface Engineering of Austenitic Stainless Steel. *Surf. Eng.* **2002**, *18*, 415–422. [CrossRef]

9. Leistikow, S.; Grabke, H.J. Effects of cold work on the oxidation behavior and carburization resistance. *Mater. Corros.* **1987**, *38*, 556–562. [CrossRef]

10. Wolf, I.; Grabke, H.J. A study on the solubility and distribution of carbon in oxides. *Solid State Commun.* **1985**, *54*, 5–10. [CrossRef]

11. Malcolm, V.T. Treatment of Steel. U.S. Patent 2,238,778A, 15 April 1941.

12. Williams, P.C.; Marx, S.V. Low Temperature Case Hardening Processes. U.S. Patent 6,461,448, 8 October 2002.

13. Christiansen, T.L.; Hummelshøj, T.S.; Somers, M.A.J. Method of Activating an Article of Passive Ferrous or Non-Ferrous Metal Prior to Carburising, Nitriding and/or Nitrocarburising. U.S. Patent 8,845,823, 30 September 2014.

14. Williams, P.C.; Marx, S.V. Low Temperature Case Hardening Processes. U.S. Patent 6,093,303A, 25 July 2000.

15. Lee, I.-S.; Barua, A. Behavior of the S-phase of Plasma Nitrocarburized 316L Austenitic Stainless Steel on Changing Pulse Frequency and Discharge Voltage at Fixed Pulse-Off Time. *Surf. Coat. Technol.* **2016**, *307*, 1045–1052. [CrossRef]

16. Christiansen, T.L.; Hummelshøj, T.S.; Somers, M.A.J. Gaseous carburising of self-passivating Fe-Cr-Ni alloys in acetylene–hydrogen mixtures. *Surf. Eng.* **2011**, *27*, 602–608. [CrossRef]

17. Ge, Y. *Low-Temperature Acetylene-Based Carburization and Nitrocarburizing of 316L Austenitic Stainless Steel*; Case Western Reserve University: Cleveland, OH, USA, 2013.

18. Ge, Y.; Ernst, F.; Kahn, H.; Heuer, A.H. The Effect of Surface Finish on Low-Temperature Acetylene-Based Carburization of 316L Austenitic Stainless Steel. *Metall. Mater. Trans. B Process. Metall. Mater. Process. Sci.* **2014**, *45*, 2338–2345. [CrossRef]

19. Gao, J.; Zhao, H.; Yang, X.; Koel, B.E.; Podkolzin, S.G. Controlling acetylene adsorption and reactions on Pt-Sn catalytic surfaces. *ACS Catal.* **2013**, *3*, 1149–1153. [CrossRef]

20. Silcocks, C.G. The Kinetics of the Thermal Polymerization of Acetylene. *Proc. R. Soc. A* **1957**, *242*, 411–429. [CrossRef]

21. Christiansen, T.L.; St, Ã.K.; Brink, B.K.; Somers, M.A.J. On the Carbon Solubility in Expanded Austenite and Formation of Hägg Carbide in AISI 316 Stainless Steel. *Steel Res. Int.* **2016**, *87*, 1–11. [CrossRef]

22. Hsieh, M.C.; Ge, Y.; Kahn, H.; Michal, G.M.; Ernst, F.; Heuer, A.H. Volatility diagrams for the Cr-O and Cr-Cl systems: Application to removal of Cr_2O_3-rich passive films on stainless steel. *Metall. Mater. Trans. B* **2012**, *43*, 1187–1201. [CrossRef]

23. Crank, J. *The Mathematics of Diffusion*; Clarendon Press: Wotton-under-edge, UK, 1975.

24. Gu, X.; Michal, G.M.; Ernst, F.; Kahn, H.; Heuer, A.H. Numerical Simulations of Carbon and Nitrogen Composition-Depth Profiles in Nitrocarburized Austenitic Stainless Steels. *Metall. Mater. Trans. A* **2014**, *45*, 4268–4279. [CrossRef]

25. Agarwala, R.P.; Naik, M.C.; Anand, M.S.; Paul, A.R.; Diffusion, D. Diffusion of carbon in stainless steels. *J. Nucl. Mater.* **1970**, *36*, 41–47. [CrossRef]

26. Wagner, C.D.; Six, H.A.; Jansen, W.T.; Taylor, J.A. Improving the accuracy of determination of line energies by ESCA: Chemical state plots for silicon-aluminum compounds. *Appl. Surf. Sci.* **1981**, *9*, 203–213. [CrossRef]

27. Hägg, G. Pulverphotogramme eines neuen Eisencarbides. *Zeitschrift für Kristallographie* **1934**, *89*, 92. [CrossRef]

28. Michal, G.M.; Ernst, F.; Heuer, A.H. Carbon Paraequilibrium in Austenitic Stainless Steel. *Metall. Mater. Trans. A* **2006**, *37*, 1819–1824. [CrossRef]

29. Villa, E.; Dagata, J.A.; Horwitz, J.; Squire, D.; Lin, M.C. Methyl radical formation from filament pyrolysis of acetylene and acetylene/hydrogen mixtures within quartz tubes. *J. Vac. Sci. Technol. A* **1990**, *8*, 3237. [CrossRef]

30. Maistro, G. Microstructural Characterization of Expanded Austenite in 304 L and 904 L Austenitic Stainless Steels. Licentiate Thesis, Department of Materials and Manufacturing Technology, Chalmers University of Technology, Gothenburg, Sweden, 2015.

31. Brink, B.K.; Ståhl, K.; Christiansen, T.L.; Oddershede, J.; Winther, G.; Somers, M.A.J. On the elusive crystal structure of expanded austenite. *Scr. Mater.* **2017**, *131*, 59–62. [CrossRef]